AD-A075 659 CATHOLIC UNIV OF AMERICA WASHINGTON D C DEPT OF PHYSICS F/G 20/11
RESONANT SCATTERING OF ELASTIC WAVES FROM SPHERICAL SOLID INCLU--ETC(U)
SEP 79 L FLAX , H UEBERALL N00014-76-C-0430

UNCLASSIFIED NL

| OF |
AD
A075659

END
DATE
FILMED
12-79
DDC

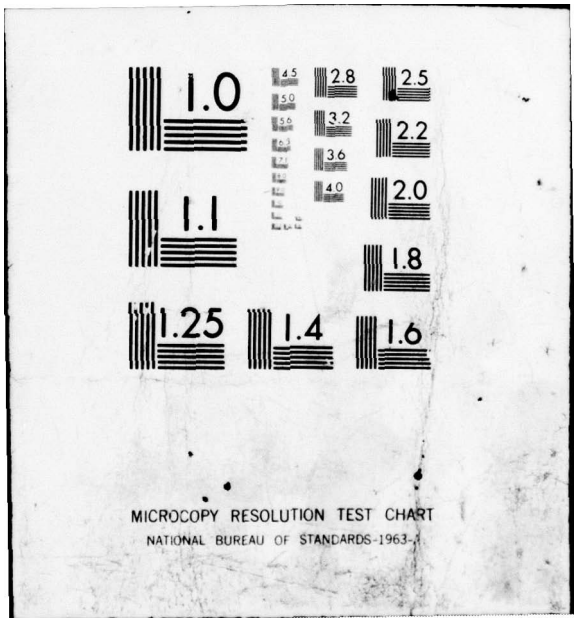
1.0
1.1
1.25
1.4
1.6
1.8
2.0
2.2
2.5
2.8
3.2
3.6
4.0
4.5
5.0
5.6
6.3
7.1
MICROCOPY RESOLUTION TEST CHART
NATIONAL BUREAU OF STANDARDS-1963-A

DEPARTMENT OF PHYSICS

The Catholic University of America

Washington, D.C. 20064

Resonant Scattering of Elastic Waves from Spherical Solid Inclusions

Lawrence Flax* and Herbert Überall+

* Naval Research Laboratory, Washington, DC 20375

+ Physics Department, Catholic University of America, Washington, DC 20064. Supported by the Office of Naval Research, Code 421.

Unclassified

SECURITY CLASSIFICATION OF THIS PAGE (When Data Entered)

REPORT DOCUMENTATION PAGE		READ INSTRUCTIONS BEFORE COMPLETING FORM
1. REPORT NUMBER	2. GOVT ACCESSION NO.	3. RECIPIENT'S CATALOG NUMBER
4. TITLE (and Subtitle) (6) Resonant scattering of Elastic Waves from Spherical Solid Inclusions.		5. TYPE OF REPORT & PERIOD COVERED Technical Report (interim) Feb.1, 1979-Jun. 31,1980
		6. PERFORMING ORG. REPORT NUMBER
7. AUTHOR(s) (10) Lawrence Flax [redacted] Herbert Uberall (15)		8. CONTRACT OR GRANT NUMBER(s) ONR N00014-76-C-0430
9. PERFORMING ORGANIZATION NAME AND ADDRESS Department of Physics Catholic University of America Washington, DC 20064		10. PROGRAM ELEMENT, PROJECT, TASK AREA & WORK UNIT NUMBERS Program 61153N, Project RR0011-08, Task RR011-008-001 Work Unit NR 384-914
11. CONTROLLING OFFICE NAME AND ADDRESS Office of Naval Research Physics Program Office Arlington, VA 22217 (11) 27 Sep 79		12. REPORT DATE September 27, 1979
		13. NUMBER OF PAGES Cover +2 p.F.1473+31p+10figs
14. MONITORING AGENCY NAME & ADDRESS(if different from Controlling Office) (12) 44		15. SECURITY CLASS. (of this report) Unclassified
		15a. DECLASSIFICATION/DOWNGRADING SCHEDULE

16. DISTRIBUTION STATEMENT (of this Report)

Approved for public release; distribution unlimited.

17. DISTRIBUTION STATEMENT (of the abstract entered in Block 20, if different from Report)

(9) Technical rept. 1 Feb 79-31 Jun 80,

18. SUPPLEMENTARY NOTES

(16) RR011 08 (17) R.R011 0801

19. KEY WORDS (Continue on reverse side if necessary and identify by block number)

Elastic-wave scattering; Resonances of Elastic Inclusions; Breit-Wigner Resonances; Regge Poles; Eigenvibrations of Elastic Objects Surface Waves; Dispersion Curves.

20. ABSTRACT (Continue on reverse side if necessary and identify by block number)

Previous investigations concerning the scattering of elastic waves from solid spherical inclusions have furnished expressions for the scattering cross sections which, upon numerical evaluation, exhibited resonance-like features as a function of frequency. In the present work, we study these resonances in a fashion suggested by the resonance theory of acoustic scattering due to Flax, Dragonette and Uberall J. Acoust. Soc. Am. 63, 723 (1978). → The resonances

DD FORM 1 JAN 73 1473 EDITION OF 1 NOV 65 IS OBSOLETE S/N 0102-LF-014-6601

Unclassified

SECURITY CLASSIFICATION OF THIS PAGE (When Data Entered)

Grant Page

076 433

of the solid inclusions, exemplified by iron or lucite spheres imbedded in an aluminum matrix, are found numerically in the individual normal-mode scattering amplitudes, and are interpreted in terms of phase-matched circumferential waves.

Dispersion curves for the phase velocities of the latter are obtained, exhibiting two families of waves of different type. Finally, the connection of these waves with the Stoneley waves on the boundary between two flat half-spaces is noted in the high-frequency limit.

Resonant Scattering of Elastic Waves from Spherical Solid Inclusions

Lawrence Flax
Naval Research Laboratory, Washington, DC 20375

and

Herbert Überall*

Physics Department, Catholic University of America, Washington, DC 20064

Abstract

Previous investigations concerning the scattering of elastic waves from solid spherical inclusions have furnished expressions for the scattering cross sections which, upon numerical evaluation, exhibited resonance-like features as a function of frequency. In the present work, we study these resonances in a fashion suggested by the resonance theory of acoustic scattering due to Flax, Dragonette and Überall [J. Acoust. Soc. Am. 63, 723 (1978)]. The resonances of the solid inclusions, exemplified by iron or lucite spheres imbedded in an aluminum matrix, are found numerically in the individual normal-mode scattering amplitudes, and are interpreted in terms of phase-matched circumferential waves.

* Supported by the Office of Naval Research, Code 421

Dispersion curves for the phase velocities of the latter are obtained, exhibiting two families of waves of different type. Finally, the connection of these waves with the Stonely waves on the boundary between two flat half-spaces is noted in the high-frequency limit.

INTRODUCTION

The scattering of plane compressional (P) or shear (S) waves by cavities or inclusions in an unbounded elastic solid medium has been investigated by a number of authors[1-15]. For example, the scattering from cylindrical obstacles has been studied for the case of empty [1] or fluid-filled[2-4] cavities, for both incident P and S waves. Scattering from ellipsoidal solid inclusions has been analyzed for P and S waves[5]. Spherical obstacles have been the object of numerous investigations: e.g., for empty spherical cavities, the scattering of P waves has been dealt with for the steady-state[6] and the transient case[7]. Scattering from fluid-filled spherical cavities was considered for incident P waves[8-10] as well as S waves [11,12]. An extensive review of the literature on elastic-wave scattering from cavities and inclusions is given in Reference 10.

For the case of scattering from solid elastic spherical inclusions, the literature contains numerical studies of scattering cross sections for incident P waves[13] and S waves[14],

based on the corresponding preceding theoretical work[15,11]. When plotting the cross sections against a dimensionless frequency variable, the authors of these studies noticed in many cases a "peaking and fluctuating" or "oscillatory behavior" of the plots, "suggesting that some type of resonance process is in effect". No detailed analysis of the resonance phenomena had been attempted at that time, however.

The present work devotes itself to such an analysis, using the recent theory of acoustic resonance scattering due to Flax, Dragonette and Überall[16]. This analysis is carried out for the case of plane compressional waves incident on spherical elastic inclusions imbedded in an unbounded elastic solid medium. (Note that a resonance study of scattering has been performed for cylindrical[3,4] and spherical fluid-filled cavities[9,10,12,17]). A similar analysis is now being carried out by us for shear waves incident on spherical elastic inclusions. Our resonance theory separates the individual ("partial wave") mode contributions into a non-resonant "geometrical" background term, and into a resonant term due to the vibrations of the inclusion. The resonant term is small off resonance, but is significant and interferes with the background at and near the resonance. The position in frequency of the resonances can be determined by solving a corresponding eigenvalue equation, which for the case of non-absorbing media is a real equation with real solutions.

We analyze numerically the cases where the scatterer is (a) a lucite sphere, and (b) an iron sphere, both imbedded in an aluminum matrix. These materials were chosen in order to provide a contrast in the corresponding background terms [approximately given by that of (a) an empty cavity, or (b) a rigid inclusion]. The resonances are obtained numerically, and are interpreted in terms of phase-matched circumferential waves. Dispersion curves for the latter are obtained, exhibiting two families of waves of different type. The connection of these surface waves with the Stoneley waves on the boundary between two flat half-spaces is noted in the high-frequency limit.

I. THEORY

The center of an elastic sphere of radius a is taken as the origin of a spherical coordinate system (r, ϑ, φ). The longitudinal and shear speeds, and the density, are designated by c_L, c_S and ρ, respectively, for the elastic matrix in which the obstacle is imbedded, and by v_L, v_S and ρ_q for the spherical obstacle itself.

The displacement vector $\vec{u}$ in either elastic material can be expressed in terms of two displacement potentials Φ and $\vec{\Psi}$, i. e

$$\vec{u} = -\vec{\nabla}\Phi + \vec{\nabla} \times \vec{\Psi} \tag{1}$$

where Φ is the scalar potential and $\vec{\Psi}$ the vector potential. Each potential satisfies a scalar wave equation. For the incident wave, we take as its solution a plane harmonic longitudinal wave propagating in the direction of the z - axis, with wave number k_L and circular frequency ω. This wave is given by $\Phi_i = \exp i(\omega t - k_L z)$ which can be expanded in spherical coordinates as

$$\Phi_i = \sum_{n=0}^{\infty} (2n+1)(-i)^n j_n(k_L r) P_n(\cos\vartheta). \qquad (2)$$

As a result of the scattering and mode conversion processes, there are both longitudinal and shear-type scattered waves, i.e.

$$\Phi_s = \sum_{n=0}^{\infty} (2n+1)(-i)^n A_n h_n^{(2)}(k_L r) P_n(\cos\vartheta) \qquad (3a)$$

(longitudinal), and

$$\Psi_s = \sum_{n=0}^{\infty} (2n+1)(-i)^n B_n h_n^{(2)}(k_s r) P_n^1(\cos\vartheta) \qquad (3b)$$

(shear), where by Ψ_s we designate the φ - component of $\vec{\Psi}_s$ which is the only nonvanishing one. The wave numbers are here $k_L = \omega/c_L$ and $k_s = \omega/c_s$; $h_n^{(2)} \equiv j_n - iy_n$ are Hankel functions of the second kind, and P_n, P_n^1 are the ordinary and associated Legendre polynomials. The undetermined coefficients A_n and B_n have to be determined from the boundary conditions at $r = a$.

Inside the scatterer, the refracted waves (labeled by a subscript q) are represented by

$$\Phi_q = \sum_{n=0}^{\infty} (2n + 1)(-i)^n C_n j_n(q_L r) P_n (\cos\vartheta) \tag{4a}$$

and

$$\Psi_q = \sum_{n=0}^{\infty} (2n + 1)(-i)^n D_n j_n(q_s r) P_n^1 (\cos\vartheta), \tag{4b}$$

where the wave numbers are $q_L = \omega/v_L$ and $q_s = \omega/v_s$.

There are four separate boundary conditions that must be satisfied by the solution to this problem. These conditions are prescribed at the interface r = a between the sphere and the matrix; they are: continuity of (i) normal (radial) and (ii) tangential displacements, and continuity of (iii) normal and (iv) tangential stresses. These are sufficient to specify the four sets of unknown coefficients A_n, B_n, C_n and D_n. Details of setting up these boundary conditions are given in the literature[18] and we shall here simply state the results.

The coefficients of the scattered waves are given as the quotients of two fourth-order determinants of the form

$$A_n = \frac{1}{\Delta} \begin{vmatrix} a_{11} & a_{12} & a_{14} & a_{15} \\ a_{21} & a_{22} & a_{24} & a_{25} \\ a_{31} & a_{32} & a_{34} & a_{35} \\ a_{41} & a_{42} & a_{44} & a_{45} \end{vmatrix} \tag{5a}$$

and

$$B_n = \frac{1}{\Delta} \begin{vmatrix} a_{11} & a_{12} & a_{13} & a_{15} \\ a_{21} & a_{22} & a_{23} & a_{25} \\ a_{31} & a_{32} & a_{33} & a_{35} \\ a_{41} & a_{42} & a_{43} & a_{45} \end{vmatrix} \tag{5b}$$

where the denominator is

$$\Delta = \begin{vmatrix} a_{11} & a_{12} & a_{13} & a_{14} \\ a_{21} & a_{22} & a_{23} & a_{24} \\ a_{31} & a_{32} & a_{33} & a_{34} \\ a_{41} & a_{42} & a_{43} & a_{44} \end{vmatrix} . \tag{5c}$$

The twenty different elements contained therein are found to be

$$a_{11} = \frac{\rho_q}{\rho} \frac{1}{1+2\xi_q} \left[j_n(Q_L) + 2\xi_q j_n''(Q_L) \right]$$

$$a_{12} = -2 \frac{\rho_q}{\rho} \frac{n(n+1)}{Q_S^2} \left[Q_S j_n'(Q_S) - j_n(Q_S) \right]$$

$$a_{13} = \frac{1}{1+2\xi} \left[h_n^{(2)}(Z_L) - 2\xi h_n^{(2)''}(Z_L) \right] \tag{6a}$$

$$a_{14} = -2 \frac{n(n+1)}{Z_S^2} \left[Z_S h_n^{(2)'}(Z_S) - h_n^{(2)}(Z_S) \right]$$

$$a_{15} = \frac{1}{1+2\xi}\left[j_n(Z_L) - 2\xi\, j_n''(Z_L) \right]$$

(from the continuity of normal stresses τ_{rr}),

$$a_{21} = Q_L\, j_n'(Q_L)$$

$$a_{22} = n(n+1)\, j_n(Q_S)$$

$$a_{23} = Z_L\, h_n^{(2)\prime}(Z_L) \qquad (6b)$$

$$a_{24} = n(n+1)\, h_n^{(2)}(Z_S)$$

$$a_{25} = Z_L\, j_n'(Z_L)$$

(from the continuity of normal displacements u_{rr}),

$$a_{31} = 2\eta\left[Q_L\, j_n'(Q_L) - j_n(Q_L) \right]$$

$$a_{32} = \eta\left[Q_S^2\, j_n''(Q_S) + (n+2)(n-1)\, j_n(Q_S) \right]$$

$$a_{33} = 2\left[Z_L\, h_n^{(2)\prime}(Z_L) - h_n^{(2)}(Z_L) \right] \qquad (6c)$$

$$a_{34} = Z_S^2\, h_n^{(2)\prime\prime}(Z_S) + (n+2)(n-1)\, h_n^{(2)}(Z_S)$$

$$a_{35} = 2\left[Z_L j_n'(Z_L) - j_n(Z_L) \right]$$

(from the continuity of tangential stresses $\tau_{r\theta}$), and

$$a_{41} = j_n(Q_L)$$

$$a_{42} = Q_S j_n'(Q_S) + j_n(Q_S)$$

$$a_{43} = h_n^{(2)}(Z_L) \qquad (6d)$$

$$a_{44} = Z_S h_n^{(2)\prime}(Z_S) + h_n^{(2)}(Z_S)$$

$$a_{45} = j_n(Z_S)$$

(from the continuity of tangential displacements u_θ).

Here, $z_L = k_L a, z_S = k_L a$, $Q_L = q_L a$, $Q_S = q_S a$,

$\xi = \mu/\lambda$, $\xi_q = \mu_q/\lambda_q$, $\eta = \mu_q/\mu$ where λ, μ are the Lamé constants of the matrix and λ_q, μ_q those of the sphere, so that

$$c_L = \left[(\lambda+2\mu)/\rho\right]^{1/2}$$
$$c_S = (\mu/\rho)^{1/2} \qquad (7a)$$

$$v_L = \left[(\lambda_2+2\mu_2)/\rho_2\right]^{1/2}$$
$$v_S = (\mu_2/\rho_2)^{1/2} . \qquad (7b)$$

This determines the coefficients of the scattered wave in terms of the incident amplitude.

The quantity of physical interest is here the differential scattering cross section as obtained, e.g., by Ying and Truell[15]. The time rate at which energy is carried away by the scattered wave across a sphere of radius $R \to \infty$ is

$$\mathcal{F} = \int (\tau_{xr}\, u_x + \tau_{yr}\, u_y + \tau_{zr}\, u_z)\, R^2 d\Omega \qquad (8a)$$

with real displacements u_i and stresses τ_{ij}. With complex fields, and going over to spherical components, this gives

$$dF = \frac{1}{2} Re\,(\tau_{rr}\, u_r^* + \tau_{r\vartheta}\, u_\vartheta^*)\, R^2 d\Omega \qquad (8b)$$

since there is no φ - dependence present. Using the well-known expressions for displacements and stresses in terms of the potentials Φ and $\vec{\Psi}$, e.g. Eq. (1), and inserting the far-field expressions of Eqs. (3a) and (3b), we find

$$dF = \frac{1}{4} i d\Omega \rho \omega^2 \left\{ \left| \sum_{n=0}^{\infty} f_n^{PP}(\vartheta) \right|^2 + \left| \sum_{n=1}^{\infty} f_n^{PS}(\vartheta) \right|^2 \right\} \quad (9a)$$

where

$$a^{-1/2} f_n^{PP}(\vartheta) = (2n+1) Z_L^{-1/2} A_n P_n(\cos\vartheta) \quad (9b)$$

$$a^{-1/2} f_n^{PS}(\vartheta) = (2n+1) Z_S^{-1/2} B_n P_n^1(\cos\vartheta). \quad (9c)$$

The total cross section σ is obtained as the integrated flux F, normalized to the flux $(i/2)\rho\omega^2 k_L$ of the incident wave, so that

$$\frac{\sigma}{\pi a^2} = 4 \sum_{n=0}^{\infty} (2n+1) \left\{ \left| \frac{A_n}{Z_L} \right|^2 + n(n+1) \frac{Z_S}{Z_L} \left| \frac{B_n}{Z_S} \right|^2 \right\}. \quad (10)$$

Note that for backscattering ($\vartheta = \pi$) there is no contribution to the scattering amplitude from the outgoing shear waves $f_n^{PS}(\pi)$ since $P_n^1(-1) = 0$.

II. RESONANCE THEORY

The resonance theory of acoustic and elastic wave scattering has been described in detail in references 16 and 9, respectively, and shall only be sketched in the present context. Using the asymptotic forms of the Hankel functions, one obtains the far-field expressions of Eqs. (3) as

$$\Phi_s \sim (i/r)(k_L a)^{-1/2} e^{-i(k_L r - \omega t)} \sum_n a^{-1/2} f_n^{PP} \qquad (11a)$$

$$\Psi_s \sim (i/r)(k_s a)^{-1/2} e^{-i(k_s r - \omega t)} \sum_n a^{-1/2} f_n^{PS} \qquad (11b)$$

together with Eqs. (9b,c). Two S-matrix elements are introduced by

$$S_n^{PP} = 1 + 2A_n \qquad (12a)$$

$$S_n^{PS} = 2B_n \qquad (12b)$$

and we find

$$S_n^{PP} = \frac{1}{\Delta} \begin{vmatrix} a_{11} & a_{12} & \hat{a}_{13} & a_{14} \\ a_{21} & a_{22} & \hat{a}_{23} & a_{24} \\ a_{31} & a_{32} & \hat{a}_{33} & a_{34} \\ a_{41} & a_{42} & \hat{a}_{43} & a_{44} \end{vmatrix} \qquad (13)$$

where $\hat{a}_{i3}$ equals $-a_{i3}$ but with $h_n^{(2)}$ replaced by $h_n^{(1)}$.

It is advantageous to consider the limit of scattering from a "soft" (i.e. evacuated) spherical cavity. This is obtained by $\rho_q \to 0$ while v_L and v_S remain constant, so that ε_q remains finite and $\eta \to 0$. (The "rigid" limit would be obtained by $\rho_q \to \infty$).

The corresponding "soft" S matrix element is thus

$$S_n^{(s)PP} = \begin{vmatrix} \hat{a}_{13} & a_{14} \\ \hat{a}_{33} & a_{34} \end{vmatrix} \Big/ \begin{vmatrix} a_{13} & a_{14} \\ a_{33} & a_{34} \end{vmatrix} \tag{14}$$

In the resonance theory[9,16], this expression is factored out of S_n^{PP} and we can write

$$S_n^{PP} = S_n^{(s)PP} \frac{\hat{G}_n}{G_n} = S_n^{(s)PP} \frac{\mathrm{Re}\,\hat{G}_n + i\,\mathrm{Im}\,\hat{G}_n}{\mathrm{Re}\,G_n + i\,\mathrm{Im}\,G_n} \tag{15a}$$

with

$$\hat{G}_n = \begin{vmatrix} a_{11} & a_{12} & \hat{a}_{13} & a_{14} \\ a_{21} & a_{22} & \hat{a}_{23} & a_{24} \\ a_{31} & a_{32} & \hat{a}_{33} & a_{34} \\ a_{41} & a_{42} & \hat{a}_{43} & a_{44} \end{vmatrix} \Big/ \begin{vmatrix} \hat{a}_{13} & a_{14} \\ \hat{a}_{33} & a_{34} \end{vmatrix}, \tag{15b}$$

and G_n a similar expression without carets. The resonances in the scattering amplitude originate from the condition (representing a real eigenvalue equation):

$$\mathrm{Re}\ G_n(Z_L) = 0, \tag{16}$$

which determines the eigenfrequencies $Z_L = Z_L^{nr}$ labeled by $r = 1,2,3\ldots$. A linear expansion of G about Z_L^{nr} then brings S_n^{PP} into an explicit resonance form:

$$S_n^{PP} = S_n^{(s)PP} \sum_{r=1}^{\infty} \frac{\mu_{nr}}{Z_L - Z_L^{nr} + i\Gamma_{nr}/2}\ , \tag{17a}$$

with a resonance width

$$\Gamma_{nr} = 2\,\mathrm{Im}\,G_n(Z_L^{nr})/\mathrm{Re}\,G_n'(Z_L^{nr}), \tag{17b}$$

and with

$$\mu_{nr} = \hat{G}_n / \mathrm{Re}\,G_n'(Z_L^{nr}). \tag{17c}$$

If Eq. (14) is written as

$$S_n^{(s)PP} = e^{2i\xi_n^{(s)}} \tag{18a}$$

with $\xi_n^{(s)}$ complex, then the quantity

$$A_n = \frac{1}{2}(S_n^{PP} - 1) \tag{18b}$$

which determines the scattered amplitude of Eq. (3a), becomes

$$\tfrac{1}{2}(S_n^{PP}-1) = \tfrac{1}{2} e^{2i\xi_n^{(s)}}\left[\sum_{r=1}^{\infty} \frac{M_{nr}^{(s)}}{Z_L - Z_L^{nr} + i\Gamma_{nr}/2}\right.$$

$$\left. + 2i e^{-i\xi_n^{(s)}} \sin\xi_n^{(s)}\right], \qquad (19a)$$

where

$$M_{nr}^{(s)} = (\hat{G}_n - G_n)/\mathrm{Re}\, G_n'(Z_L^{nr}). \qquad (19b)$$

This shows that the scattering amplitude consists of a non-resonant background term [the second term in brackets in Eq. (19a)] which is due to the scattering of P waves from a soft sphere, with a series of superimposed resonances (first term in brackets) which will interfere with the background amplitude. A corresponding expression may be derived for B_n of Eqs. (3b) and (12a), i.e. the mode-converted scattering amplitude:

$$\tfrac{1}{2} S_n^{PS} = \tfrac{1}{2} e^{2i\xi_n^{(s)}} \left\{ \sum_{r=1}^{\infty} \frac{\tilde{M}_{nr}^{(s)}}{Z_L - Z_L^{nr} + i\Gamma_{nr}/2} + 1 \right\}. \qquad (19c)$$

Note that the resonance frequencies are here the same as in Eq. (19a) since the resonances are due to the vibrations of the same inclusion in both cases, independent of the resonance mechanism.

The expressions of Eqs. (19a), (19c) hold in the framework of the resonance approximation, valid if the width of the resonances is saml1 compared to their spacing. However, the actual numerical calculations to be discussed below have all been carried out using the exact expressions Eqs. (5).

III. NUMERICAL RESULTS

Scattering amplitudes have be evaluated numerically for the cases of (a) a lucite sphere, and (b) an iron sphere, both imbedded in an aluminum matrix. The material parameters of these substances (assumed non-absorptive) are listed in Table I.

In Fig. 1a, we plot for case (a), lucite in aluminum, the amplitude moduli $a^{-1/2}|f_n^{PP}|/P_n(\cos\vartheta)$ of Eq. (9b) vs. $k_L a \equiv Z_L$

of aluminum, for the partial waves n = 0, 1 and 2. Similarly,

Fig. 1b shows the quantity $a^{-1/2}\,|f_n^{PS}|\,/P_n^1(\cos\vartheta)$ of Eq. (9c), i.e. the mode-converted scattering amplitude. In both cases, the interference pattern of the resonances of the lucite sphere with a non-resonant background is clearly visible. Due to the much smaller impedances of the lucite sphere ($\rho_2 v_L$, $\rho_2 v_S$) as compared to those of the aluminum matrix (ρc_L , ρc_S), it is expected that the background resembles closely that of scattering from an empty cavity in aluminum. We therefore plot in Figs. 2a and 2b the quantities $a^{-1/2}\,|f_n^{PP} - f_n^{(s)PP}|\,/P_n$ and $a^{-1/2}\,|f_n^{PS} - f_n^{(s)PS}|\,/P_n^1$, respectively, where the "soft" background amplitudes $f_n^{(s)PP}$ or $f_n^{(s)PS}$, obtained from Eqs. (9b), (9c) in the limit $\rho_2 \to 0$, were subtracted out from the total partial-wave amplitudes. Indeed, the pure resonances of the cavity contents appear to have been made visible in this way. The resonance frequencies are the same in both cases, but it is seen that two families of resonances are present, and only one of these is being excited in P → P scattering while both families are excited in P → S scattering.

Similar numerical results are shown for case (b), iron in aluminum, where the n = 0, 1 and 2 partial wave scattering amplitude moduli are shown for P → P scattering in Fig. 3a, and for P → S scattering in Fig. 3b. Due to the density of the

inclusion being larger than that of the matrix, the background is now expected to correspond to scattering from a rigid sphere ($\rho/\rho_2 \to 0$). In fact if this background is subtracted from f_n^{PP} or f_n^{PS} and the modulus is taken subsequently, Figs. 4a (P → P scattering) and 4b (P → S scattering) indicate that the pure resonance amplitudes are indeed obtained in this way. (The resonance formulation with a rigid background is similar to that for the soft background given in Section II, see, e.g. references 9 and 16).

From Figs. 2 and 4, the resonance frequencies for cases (a) and (b) may be read off and tabulated. They may serve to obtain the dispersion curves of circumferential waves propagating over the surface of the inclusion, which have been shown to be generated during the scattering process, and to provide an interpretation for the existence of the resonances[10,19].

The resonance frequencies $\mathcal{Z}_L^{nr}$ in the resonance expression for the S - matrix, Eq. (17a), are functions of the mode number n which we now consider a continuous variable. We may expand $\mathcal{Z}_L^{nr}$ in the n- variable about the value $n = n_r$, chosen so that $\mathcal{Z}_L^{n_r r} = \mathcal{Z}_L$ (the incident frequency):

$$\mathcal{Z}_L^{nr} = \mathcal{Z}_L^{n_r r} + (n - n_r)\left(d\mathcal{Z}_L^{nr}/dn\right)_{n=n_r} . \qquad (20)$$

Inserting into Eq. (17a) brings the latter into the form

$$S_n^{PP} = S_n^{(s)PP} \sum_{r=1}^{\infty} \frac{\hat{\mu}_{nr}}{n - n_r - i\hat{\Gamma}_{nr}/2} \tag{21a}$$

where

$$\hat{\mu}_{nr} = -\mu_{nr} \,/\, (dZ_L^{nr}/dn)_{n=n_r}, \tag{21b}$$

and where the width in the n - domain is

$$\hat{\Gamma}_{nr} = \Gamma_{nr} \,/\, (dZ_L^{nr}/dn)_{n=n_r}. \tag{21c}$$

Eq. (21a) is an expression which has "Regge" poles in the complex n - plane, located at

$$\hat{n}_r = n_r + i\hat{\Gamma}_{nr}/2. \tag{21d}$$

They may be utilized for an evaluation of the scattering amplitude, Eq. (3a), in terms of the Watson transformation[10,19] with the result that the outgoing portion of the total $P \to P$ scattering amplitude has the asymptotic form[19]

$$\Phi \to 2\pi \sum_{r=1}^{\infty} \sum_{m=0}^{\infty} \sum_{\varepsilon=\pm} \left(\frac{2}{\pi(\hat{n}_r + \frac{1}{2}) \sin\vartheta} \right)^{1/2} (2\hat{n}_r + 1)\, \hat{\Gamma}_{nr}$$

$$\times \exp i\left[2\xi_{\hat{n}_r}^{(s)} - \pi \hat{n}_r/2 + (2m+1)\pi \hat{n}_r + \varepsilon(\hat{n}_r + \tfrac{1}{2})(\pi - \vartheta) - \varepsilon\pi/4 \right]. \quad (22)$$

This describes a manifold (labeled by r) of attenuated circumferential "tidal" waves which engulf the spherical inclusion along all meridians (m = o), with additional components ($m > 0$) that have previously circumnavigated the inclusion m times. The phase velocity of the rth surface wave is given by

$$c_r(Z_L) = \frac{Z_L c_L}{n_r + \frac{1}{2}} . \quad (23)$$

When the Regge pole of Eq. (21d), which with varying frequency moves through the complex n - plane along a "Regge trajectory", passes by the integer n so that $n_r \to n$, the wavelength of a surface wave,

$$\lambda_r(Z_L) = 2\pi a / (n_r + \tfrac{1}{2}), \quad (24)$$

becomes $2\pi a/(n+\frac{1}{2})$ so that $n + \frac{1}{2}$ wavelengths span the circumference of the spherical inclusion. Since as seen from Eq.(22), the circumferential wave suffers a phase loss of $\pi/2$ (i.e., a quarter wavelength) every time it passes through one of the convergence points $\vartheta = 0, \pi$ at the north and south pole of the spherical inclusion, this condition leads to a perfect phase

match of the wave after each circumnavigation. The poles in the scattering amplitude, Eqs. (17a) or (21a), therefore describe a "resonant buildup" of the amplitude of the circumferential wave in the course of its repeated circumnavigations due to phase matching, which becomes physically manifest at the integer mode amplitudes, leading to the resonances shwon, e.g., in Figs.2 or 4. The families of resonances which in these figures are manifest in all partial-wave amplitudes and which recur at successively higher frequencies in successive partial waves, each thus correspond to, and represent, one single circumferential wave. In a sense, this physical picture (which applies generally to any type of smooth spherical scatterer), explains the existence of the scatterer's resonances in terms of a phase matching of the circumferential waves which its surface may support.

Using the resonance frequencies which appear in Figs. 2 and 4, (as well as in corresponding graphs for higher partial waves), we may obtain dispersion curves of the surface waves from Eq. (23). These are shown in Fig. 5 (for lucite in aluminum) and Fig. 6 (for iron in aluminum), where the quantity c_r/c_L is plotted vs. Z_L for all the surface waves labeled by r. From these dispersion curves, we see that the surface waves on an elastic spherical inclusion imbedded in an elastic medium fall into two classes (represented in Figs. 5 and 6 by solid and

dashed curves, respectively), which presumably correspond to longitudinal and shear type surface waves. The distinction between these two classes of curves, when producing the plots, has been greatly facilitated by the fact that in P → P scattering (Figs. 2a and 4a) only one class of surface waves seems to have been excited, while in P → S scattering (Figs. 2b and 4b), both are excited. For small values of Z_L, however, the distinction in the excitation mechanism, and hence in the dispersion curves, is no longer so clear-cut.

At the end, we would like to comment on the high-frequency (or large-a) limit of the dispersion curves, $Z_L \to \infty$. In this limit, the dispersion curves approach horizontal asymptotic values, while physically, the boundary of the inclusion tends towards the flat boundary between two infinite elastic half-spaces. In that latter case, the speed of surface waves on the boundary, c, satisfies the Stoneley equation[20]

$$c^4\left[(\rho-\rho_2)^2+(\rho M_2+\rho_2 M)(\rho N_2+\rho_2 N)\right]$$
$$+2Rc^2(\rho M_2 N_2-\rho_2 MN-\rho+\rho_2) \qquad (25$$
$$+R^2(MN-1)(M_2N_2-1)=0$$

where

$$M = (1 - c^2/c_L^2)^{1/2}$$

$$M_q = (1 - c^2/v_L^2)^{1/2}$$

$$N = (1 - c^2/c_S^2)^{1/2} \qquad (25b)$$

$$N_q = (1 - c^2/v_S^2)^{1/2}$$

$$R = 2(\rho c_S^2 - \rho_q v_S^2).$$

We have solved this equation numerically, and have found a Stoneley root $c/c_L = 0.504$ for the case of iron in aluminum; no root was found for the case of lucite in aluminum. (It is well-known[20] that Stoneley wave solutions do not always exist on the flat boundary between two elastic half-spaces).

In Fig. 5, we have entered two arrows on the right-hand side representing the values $v_L/c_L = 0.4080$ and $v_S/c_L = 0.2010$. While many of the dispersion curves on this graph fall below v_L/c_L for large enough Z_L, the value v_S/c_L is found to represent a comfortable lower limit for even the lowest dispersion curve, up to the largest Z_L- value ($Z_L = 25$) at which that dispersion curve was obtained; but this value was not yet large enough to decide whether v_S/c_L actually constitutes an asymptote for the dispersion curves.

In Fig. 6, we have entered three arrows representing the values (from top) $v_L/c_L = 0.8815$, $c/c_L = 0.504$ (the Stoneley wave solution), and $v_s/c_L = 0.4720$. While either of the two latter values seems to represent an asymptote to the dispersion curves on this figure, a plot of the lowest dispersion curve up to $Z_L = 35$ reveals that at $Z_L = 24$, this curve falls below the value of c/c_L, but that the value of v_s/c_L represents a likely asymptote for the lowest dispersion curve. Since in this case of iron in aluminum, the higher dispersion curves lie considerably above the lowest one, no statements could be made about their asymptotics, except that several of them definitely fall below the value of v_L/c_L as Z_L increases.

IV. CONCLUSION

This work represents the first systematic study of resonance effects in the scattering of elastic (P) waves from solid spherical inclusions. The resonance approach is patterned after our previous resonance studies in acoustic scattering[16], and in elastic-wave scattering from fluid-filled cavities[9,10]. Both in that latter case, and in the present case, the resonances are caused by the vibration of the substance filling the cavity, and they can be shown to originate from the phase-matching, or

resonant reinforcement, of repeatedly circumnavigating surface waves. But while in the case of a fluid-filled cavity only one type of surface wave has been found[9,10], the present case of a solid inclusion is endowed with two different classes of surface waves, as evident from their dispersion curves which were obtained here. It is interesting to note that P → P scattering (without mode conversion) only sets up one of these two classes of surface waves, while P → S scattering (with mode conversion) excites both classes. The asymptotic behavior for high frequencies of the dispersion curves has been compared with the Stoneley wave limits for two half-spaces in contact, and it was found, at least for the case of an iron inclusion in aluminum, that the Stoneley wave speed does not represent an asymptote of the lowest dispersion curve while the shear speed of iron probably does. In the lucite-aluminum case, again the shear speed of Lucite probably represents the asymptote of some of the dispersion curves.

TABLE I

Material Parameters Used

Material	density $x10^{-3} kg/m^3$	Longitudinal speed $x\ 10^{-3} m/sec$	Shear speed $x\ 10^{-3} m/sec$
Aluminum	2.7	6.568	3.149
Iron	7.7	5.79	3.10
Lucite	1.182	2.68	1.38

REFERENCES

1. L. Flax and W. G. Neubauer, "Reflection of elastic waves by a cylindrical cavity in an absorptive medium", J. Acoust. Soc. Am. 63, 675 (1978)

2. Y. H. Pao and C. C. Mow, "Theory of normal modes and ultrasonic spectral analysis of the scattering of waves in solids", J. Acoust. Soc. Am. 59, 1046 (1976)

3. A. J. Haug, S. G. Solomon, and H. Überall, "Resonance theory of Elastic Wave Scattering from a Cylindrical Cavity", J. Sound.Vib. 57, 51 (1978)

4. S. G. Solomon and H. Überall, "Mode Conversion and Resonance Scattering of elastic waves from a cylindrical fluid-filled cavity", to be submitted to J. Acoust. Soc. Am.

5. S. K. Datta, "Diffraction of plane elastic waves by ellipsoidal inclusions", J. Acoust. Soc. Am. 61, 1432 (1977)

6. B. R. Tittmann, E. R. Coehn, and J. M. Richardson, "Scattering of Longitudinal waves incident on a spherical cavity in a solid", J. Acoust. Soc. Am. 63, 68 (1978)

7. F. R. Norwood and J. Miklowitz, "Diffraction of transient elastic waves by a spherical cavity", J. Appl. Mech. 34, 735 (1967)

8. N. G. Einspruch and R. Truell, "Scattering of a plane longitudinal wave by a spherical fluid obstacle in an elastic medium", J. Acoust. Soc. Am. 32, 214 (1960)

9. G. Gaunaurd and H. Überall, "Theory of resonant scattering from spherical cavities in elastic and viscoelastic media", J. Acoust. Soc. Am. 63, 1699 (1978)

10. G. C. Gaunaurd and H. Überall, "Numerical evaluation of modal resonances in the echoes of compressional waves scattered from fluid-filled spherical cavities in solids", J. Appl. Phys. (in press)

11. N. G. Einspruch, E. J. Witterholt, and R. Truell, "Scattering of a plane transverse wave by a spherical obstacle in an elastic medium", J. Appl. Phys. 31, 806 (1960)

12. D. Brill, G. Gaunaurd and H. Überall, "Resonance theory of elastic wave scattering from spherical fluid obstacles in solids", submitted to J. Acoust. Soc. Am.

13. G. Johnson and R. Truell, "Numerical computations of elastic scattering cross sections", J. Appl. Phys. 36, 3466 (1965)

14. R. J. McBride and D. W. Kraft, "Scattering of a transverse elastic wave by an elastic sphere in a solid medium", J. Appl. Phys. 43, 4853 (1972)

15. C. F. Ying and R. Truell, "Scattering of a plane Longitudinal wave by a spherical obstacle in an isotropically elastic solid", J. Appl. Phys. 27, 1086 (1956)

16. L. Flax, L. R. Dragonette, and H. Überall, "Theory of elastic resonance excitation by sound scattering", J. Acoust. Soc. Am. 63, 723 (1978)

17. G. Gaunaurd, K. P. Scharnhorst, and H. Überall, "Giant monopole resonances in the scattering of waves from gas-filled spherical cavities and bubbles", J. Acoust. Soc. Am. 65, 573, (1979)

18. See, e.g., Y. H. Pao and C. C. Mow, "Diffraction of Elastic Waves and Dynamic Stress Concentrations", Crane and Russak Co., New York, 1972.

19. J. D. Murphy, J. George, A. Nagl and H. Überall, "Isolation of the resonant component in acoustic scattering from fluid-loaded elastic spherical shells", J. Acoust. Soc. Am. 65, 368 (1979).

20. See, e.g., W. M. Ewing, W. S.Jardetzky and F. Press, "Elastic Waves in Layered Media", McGraw Hill, New York, 1957.

FIGURE CAPTIONS

Fig. 1. Plot of (a) $a^{-1/2}|f_n^{PP}|/P_n(\cos\vartheta)$, and (b) $a^{-1/2}|f_n^{PS}|/P_n^1(\cos\vartheta)$ vs. Z_L for the partial waves n = o, 1, and 2, case of a Lucite sphere in aluminum.

Fig. 2. Plot of (a) $a^{-1/2}|f_n^{PP}-f_n^{(s)PP}|/P_n(\cos\vartheta)$ and (b) $a^{-1/2}|f_n^{PS}-f_n^{(s)PS}|/P_n^1(\cos\vartheta)$ vs. Z_L (where $f_n^{(s)}$ is the empty-cavity scattering amplitude) for the partial waves n = o, 1, and 2, case of a lucite sphere in aluminum.

Fig. 3. Plot of (a) $a^{-1/2}|f_n^{PP}|/P_n(\cos\vartheta)$, and (b) $a^{-1/2}|f_n^{PS}|/P_n^1(\cos\vartheta)$ vs. Z_L for the partial waves n = o, 1, and 2, case of an iron sphere in aluminum.

Fig. 4. Plot of (a) $a^{-1/2}|f_n^{PP}-f_n^{(r)PP}|/P_n(\cos\vartheta)$ and (b) $a^{-1/2}|f_n^{PS}-f_n^{(r)PS}|/P_n^1(\cos\vartheta)$ vs. Z_L (where $f_n^{(r)}$ is the rigid-inclusion scattering amplitude) for the partial waves n = 0, 1, and 2, case of an iron sphere in aluminum

Fig. 5. Dispersion curves for the two families of surface waves on a lucite sphere in aluminum. Arrows on the right represent the values $v_L/c_L = 0.4080$ and $v_S/c_L = 0.2010$.

Fig. 6. Dispersion curves for the two families of surface waves on an iron sphere in aluminum. Arrows on the right represent the values $v_L/c_L = 0.8815$, $c/c_L = 0.504$ (the Stoneley wave speed), and $v_S/c_L = 0.4720$

Fig. 1a

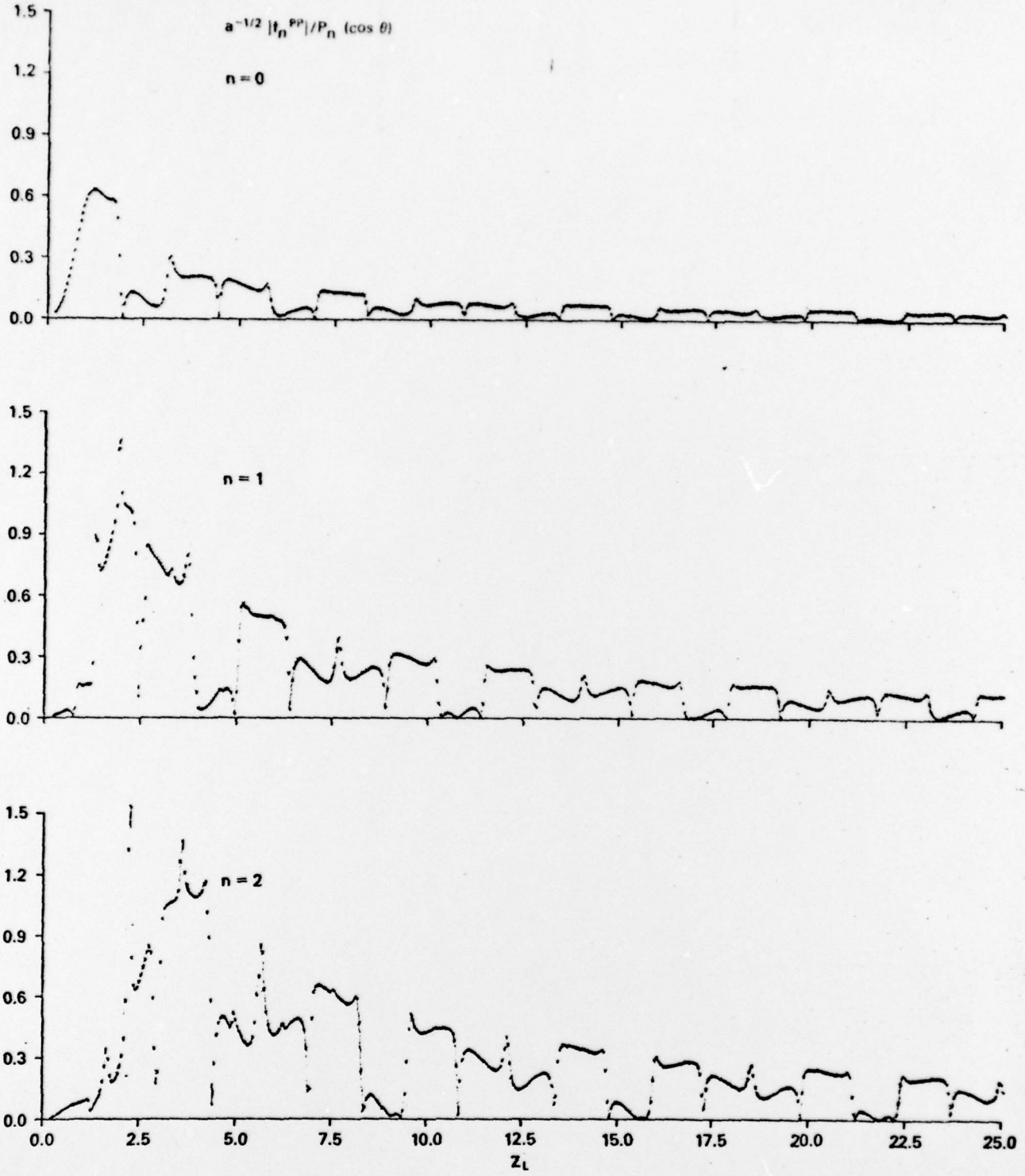
$a^{-1/2} |t_n^{PP}|/P_n$ (cos θ)
n = 0
n = 1
n = 2
1.5
1.2
0.9
0.6
0.3
0.0
0.0
2.5
5.0
7.5
10.0
12.5
15.0
17.5
20.0
22.5
25.0
z_L

Fig. 1b

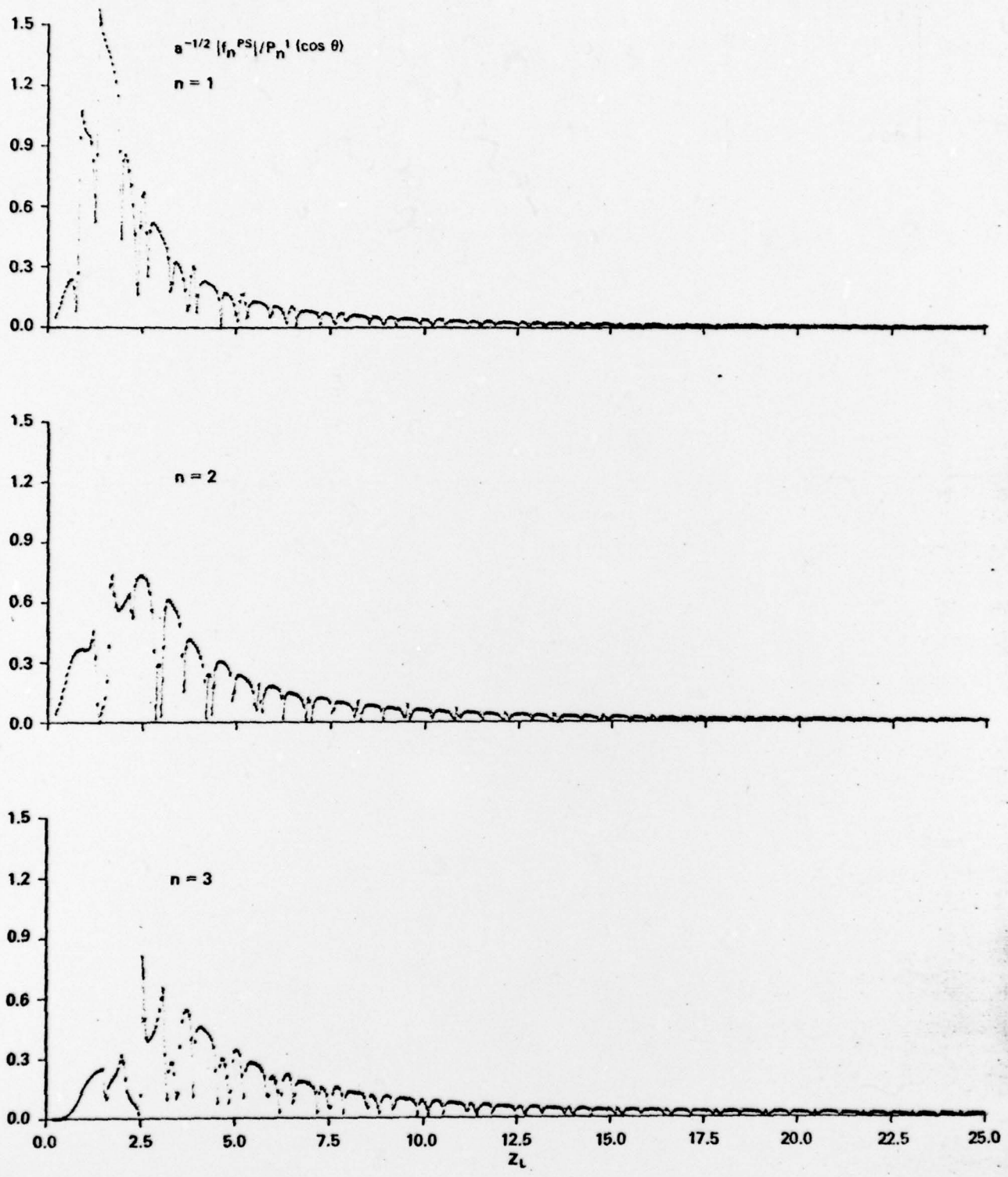
$a^{-1/2} |f_n^{PS}|/P_n^1 (\cos\theta)$
n = 1
n = 2
n = 3
1.5
1.2
0.9
0.6
0.3
0.0
0.0
2.5
5.0
7.5
10.0
12.5
15.0
17.5
20.0
22.5
25.0
z_L

Fig. 2a

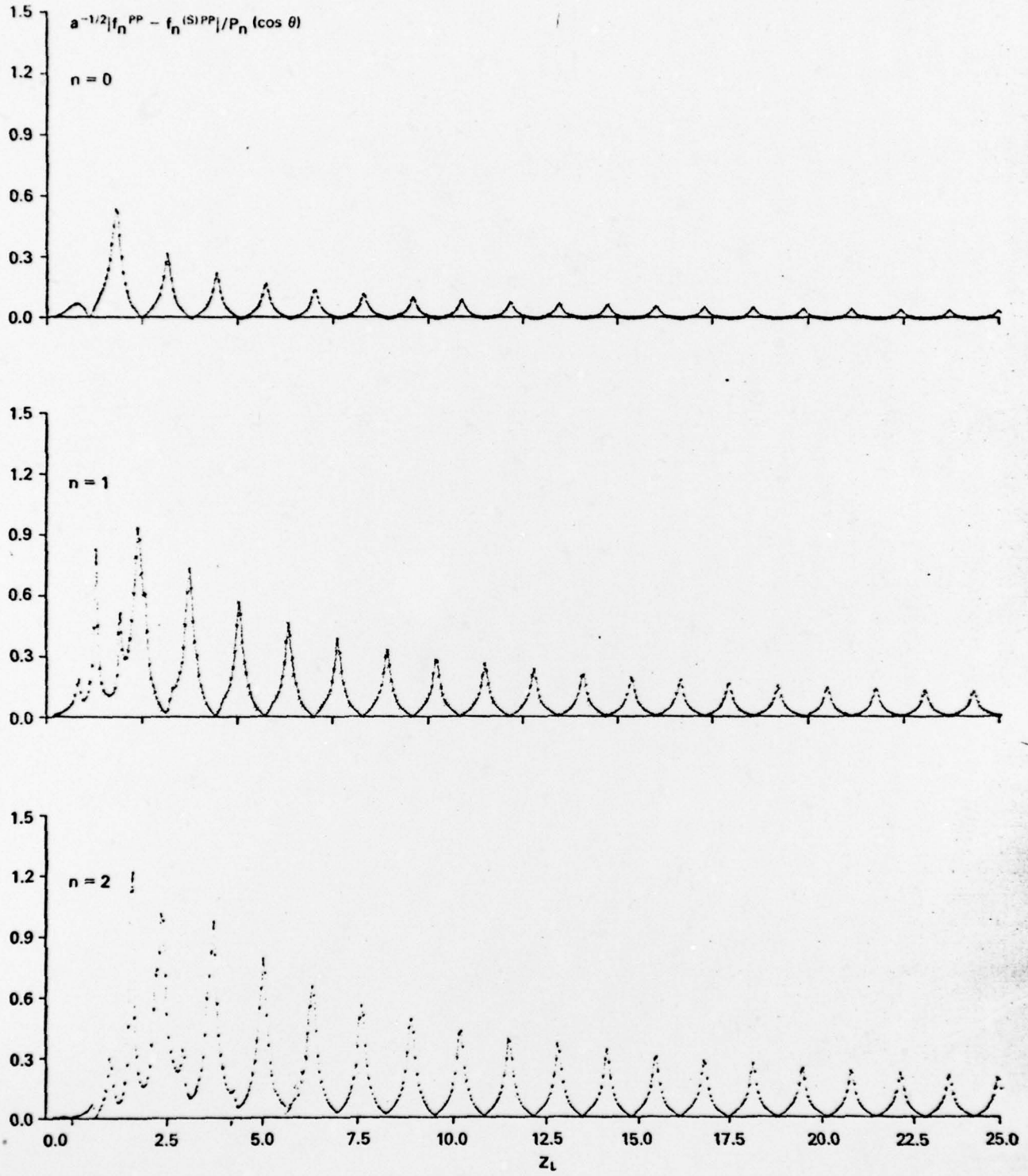
$a^{-1/2}|f_n^{PP} - f_n^{(S)PP}|/P_n(\cos\theta)$
n = 0
n = 1
n = 2
1.5
1.2
0.9
0.6
0.3
0.0
0.0
2.5
5.0
7.5
10.0
12.5
15.0
17.5
20.0
22.5
25.0
z_L

Fig. 2b

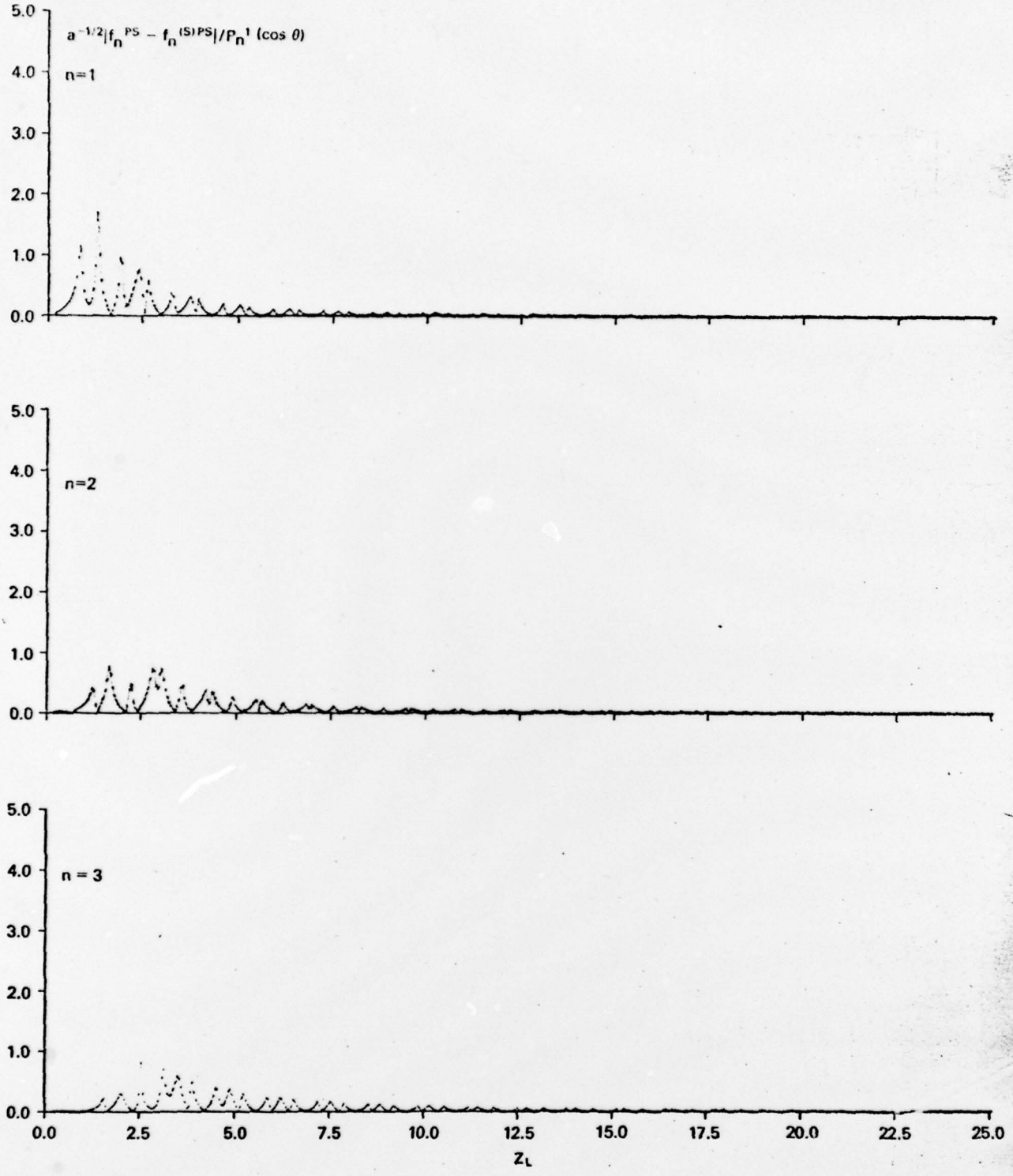
$a^{-1/2}|f_n^{PS} - f_n^{(S)PS}|/P_n^1(\cos\theta)$
n=1
n=2
n = 3
5.0
4.0
3.0
2.0
1.0
0.0
0.0
2.5
5.0
7.5
10.0
12.5
15.0
17.5
20.0
22.5
25.0
z_L

Fig. 3a

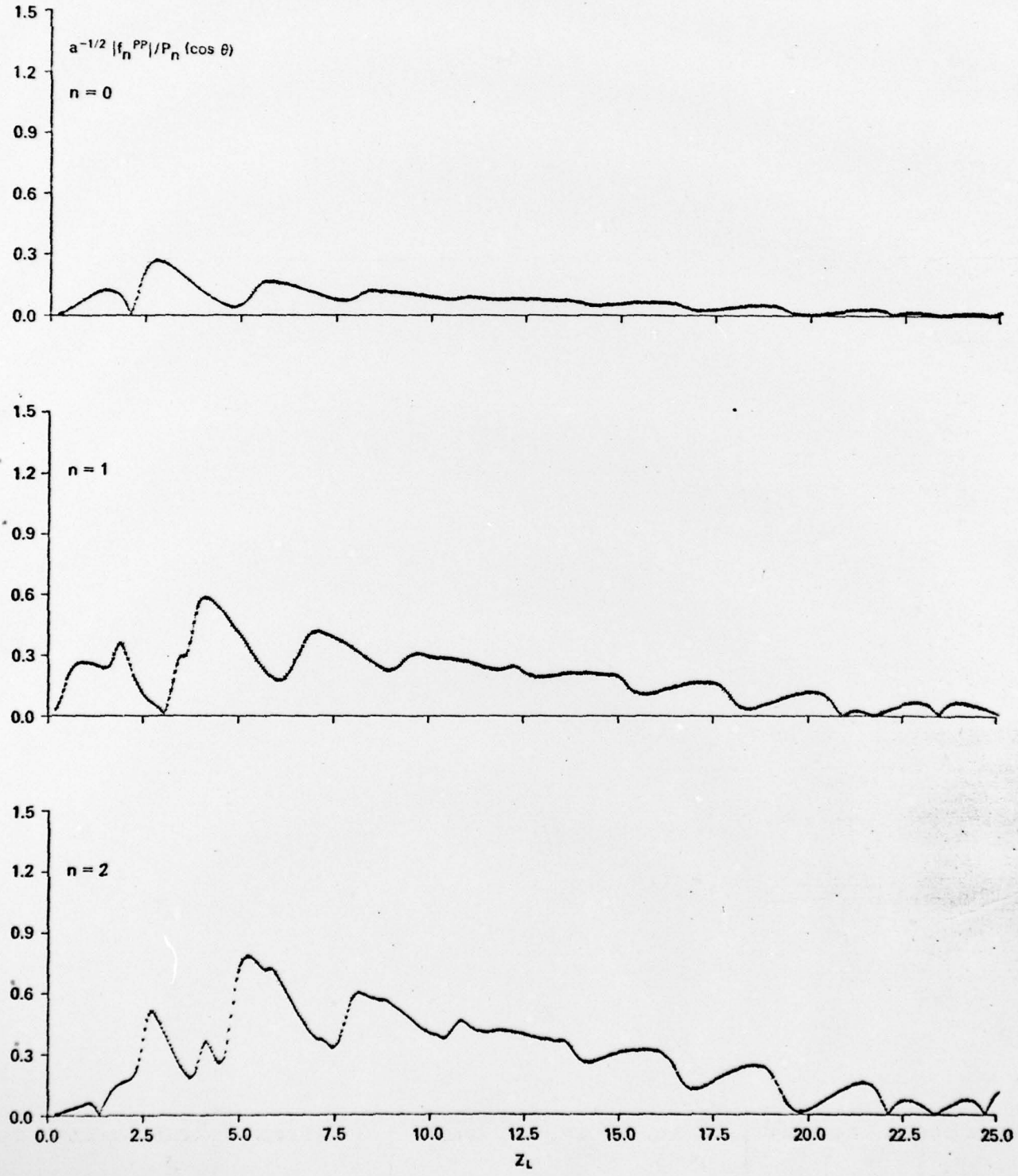
$a^{-1/2} |f_n^{PP}|/P_n (\cos\theta)$
n = 0
n = 1
n = 2
1.5
1.2
0.9
0.6
0.3
0.0
0.0
2.5
5.0
7.5
10.0
12.5
15.0
17.5
20.0
22.5
25.0
Z_L

Fig. 3b

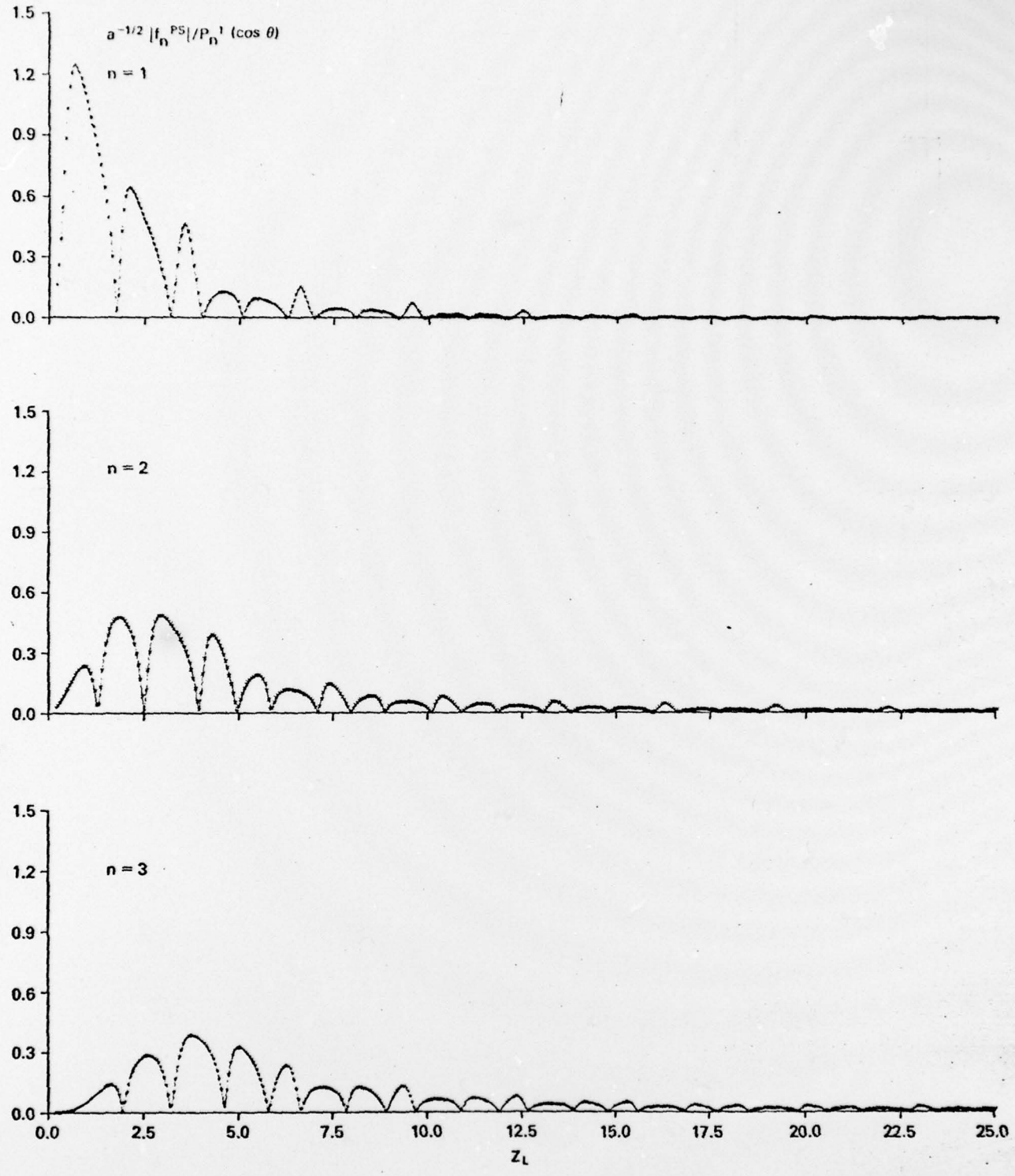
$a^{-1/2} |f_n^{PS}|/P_n^1 (\cos\theta)$
n = 1
n = 2
n = 3
1.5
1.2
0.9
0.6
0.3
0.0
0.0
2.5
5.0
7.5
10.0
12.5
15.0
17.5
20.0
22.5
25.0
Z_L

Fig. 4a

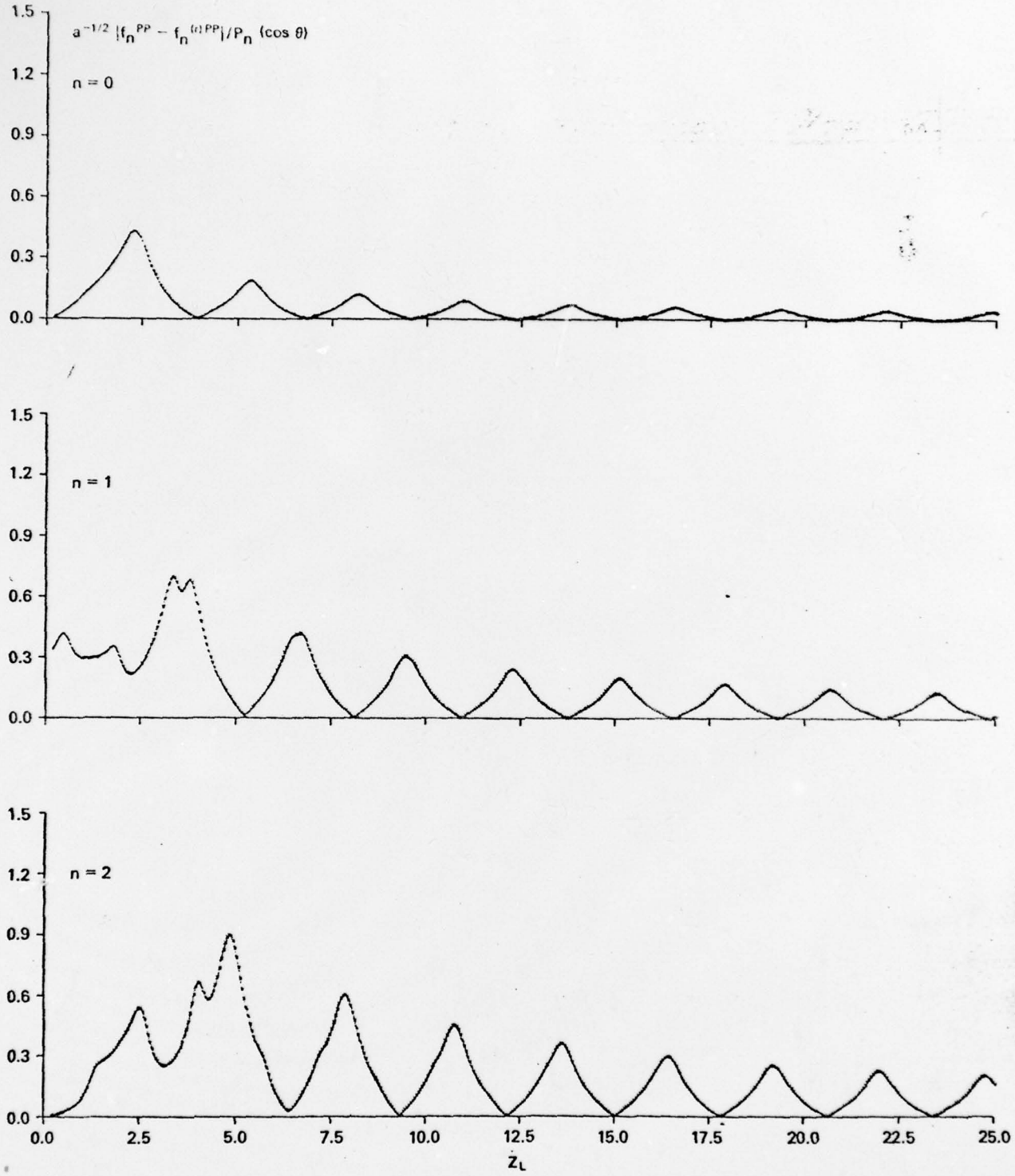
$a^{-1/2}\,|f_n^{PP} - f_n^{(a)PP}|/P_n\,(\cos\theta)$
n = 0
n = 1
n = 2
1.5
1.2
0.9
0.6
0.3
0.0
0.0
2.5
5.0
7.5
10.0
12.5
15.0
17.5
20.0
22.5
25.0
z_L

Fig. 4b

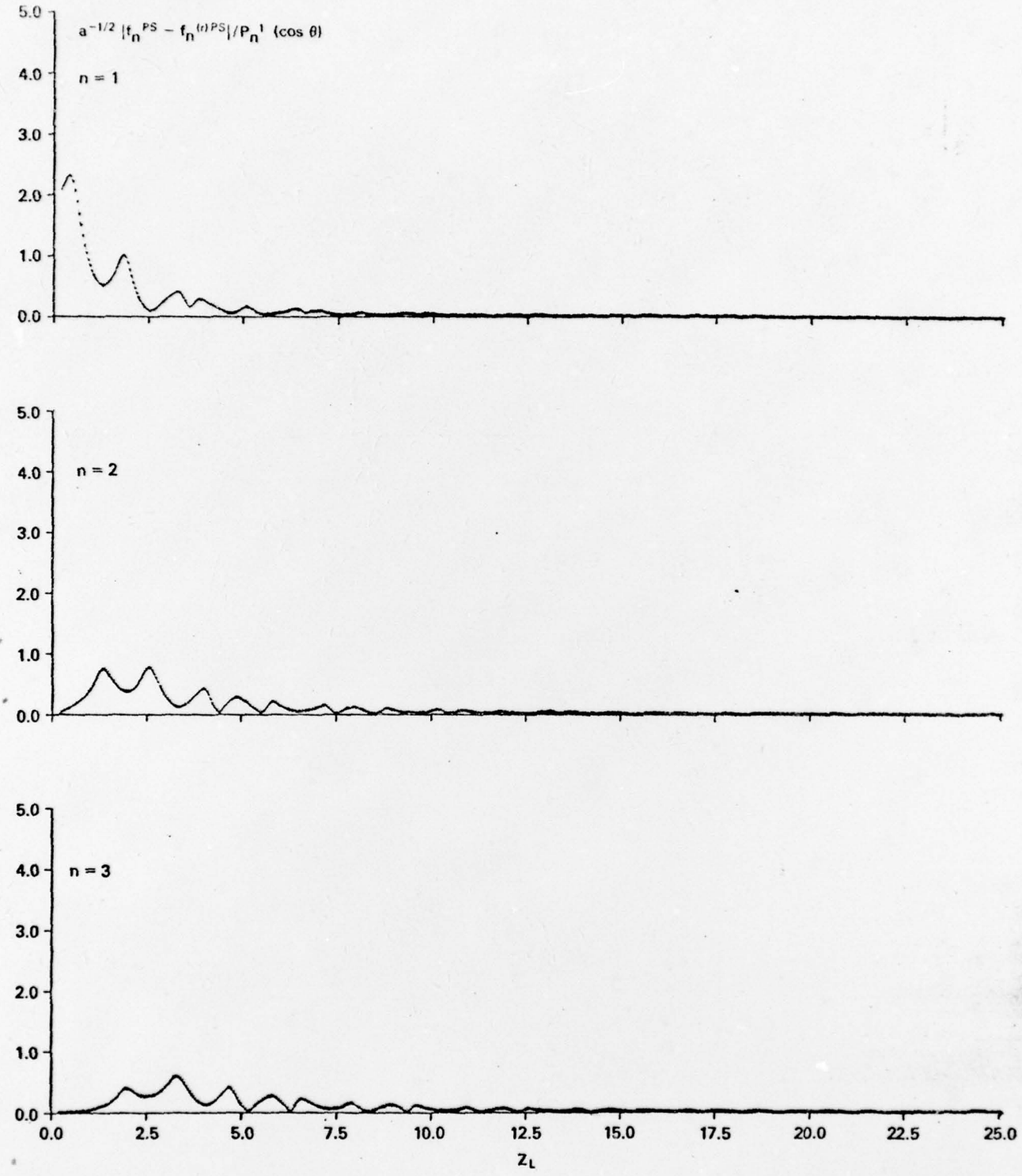
$a^{-1/2} |f_n^{PS} - f_n^{(n)PS}|/P_n^1 (\cos\theta)$
n = 1
n = 2
n = 3
5.0
4.0
3.0
2.0
1.0
0.0
0.0
2.5
5.0
7.5
10.0
12.5
15.0
17.5
20.0
22.5
25.0
Z_L

Fig. 5

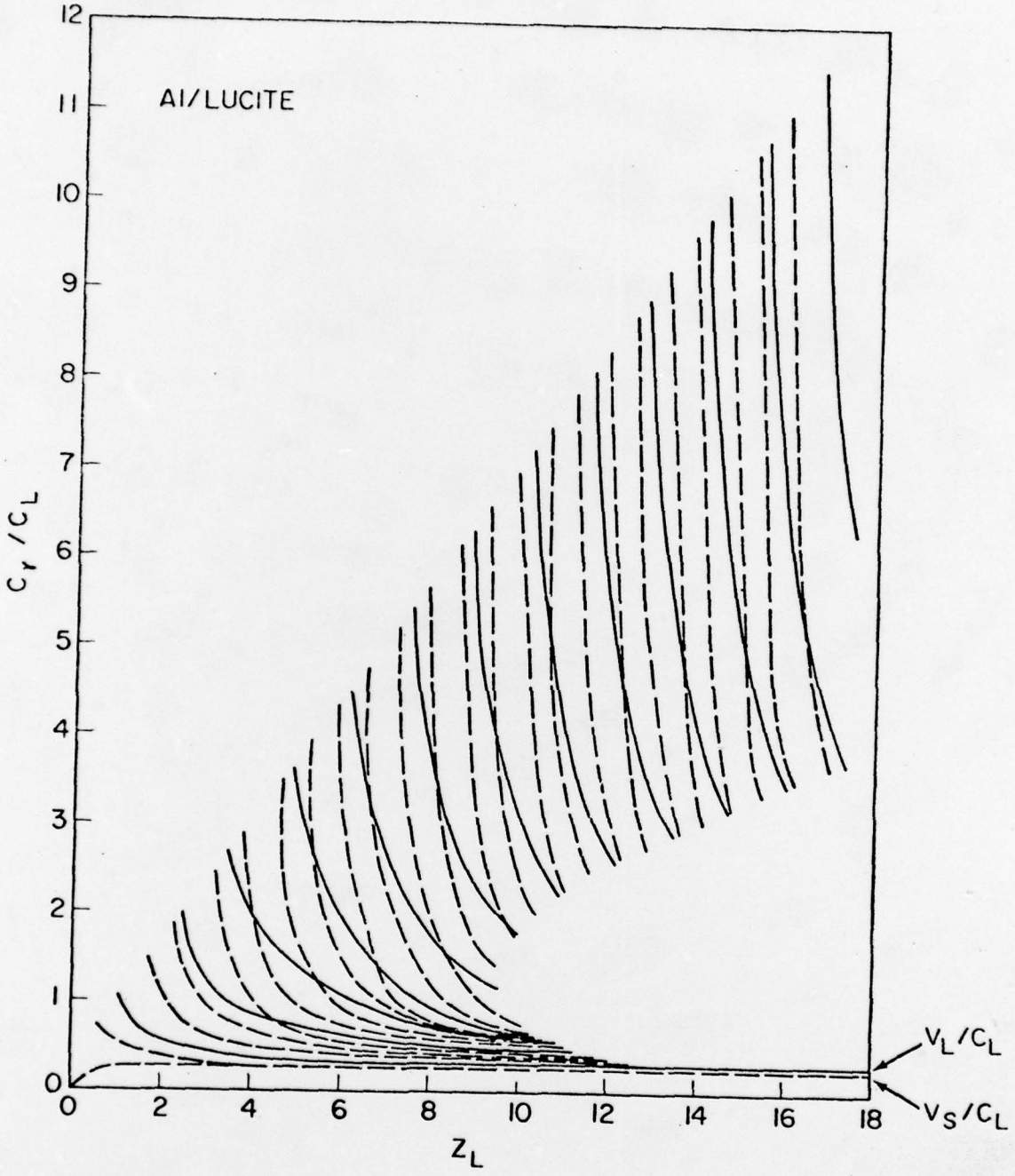
AI/LUCITE
C_r/C_L
Z_L
V_L/C_L
V_S/C_L
0
1
2
3
4
5
6
7
8
9
10
11
12
0
2
4
6
8
10
12
14
16
18

Fig. 6

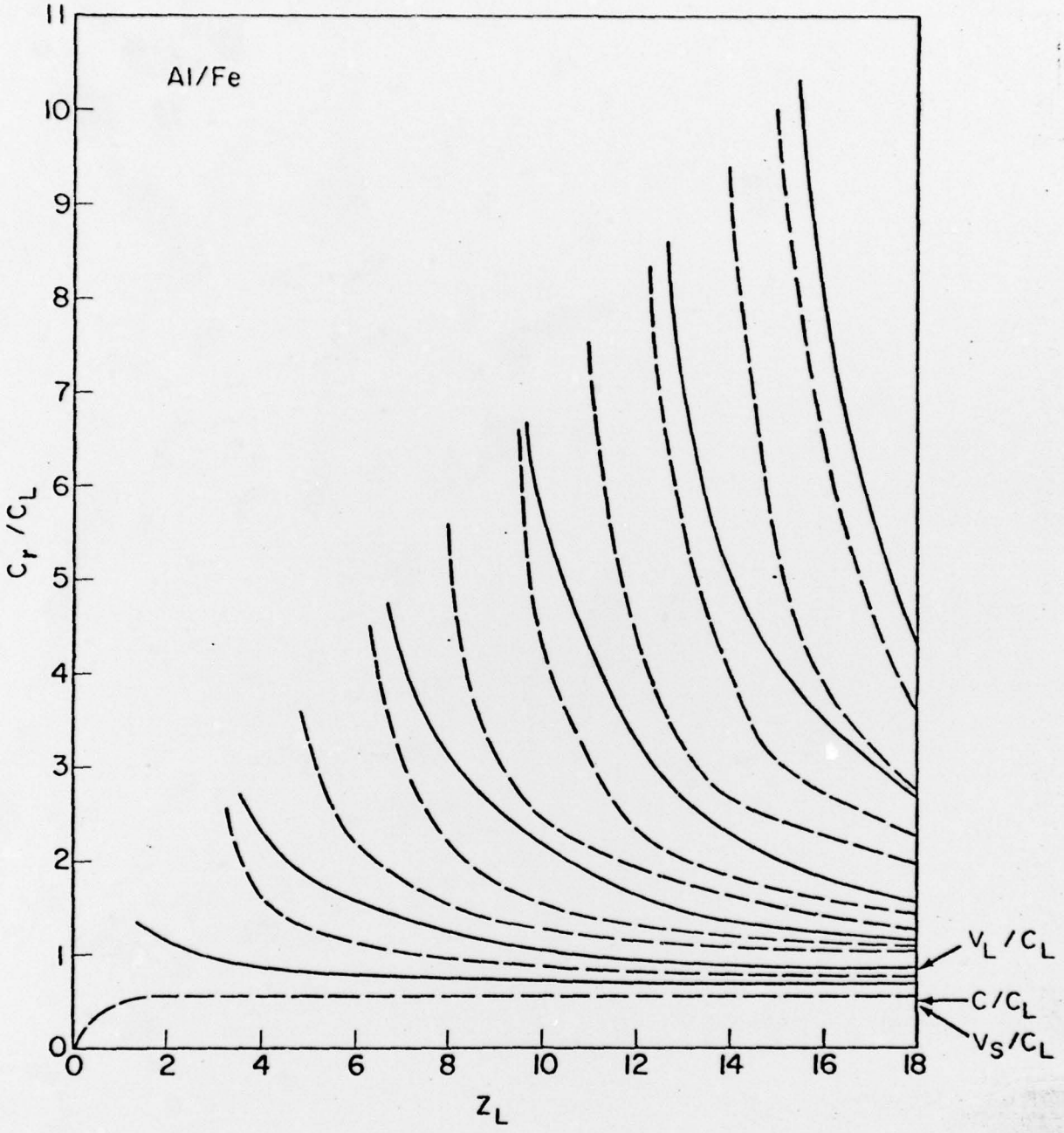
Al/Fe
C_r / C_L
Z_L
V_L / C_L
C / C_L
V_S / C_L
0
1
2
3
4
5
6
7
8
9
10
11
0
2
4
6
8
10
12
14
16
18